Editors' Suggestion | Featured in Physics

# Entropic Costs of Extracting Classical Ticks from a Quantum Clock

Vivek Wadhia,[1,*,†] Florian Meier,[2,*,‡] Federico Fedele,[1] Ralph Silva,[3] Nuriya Nurgalieva,[4] David L. Craig,[5] Daniel Jirovec,[6] Jaime Saez-Mollejo,[6] Andrea Ballabio,[7] Daniel Chrastina,[7] Giovanni Isella,[7] Marcus Huber,[2,8] Mark T. Mitchison,[9,10] Paul Erker,[2,8] and Natalia Ares[1,§]

[1]*Department of Engineering Science, University of Oxford, Parks Road, Oxford OX1 3PJ, United Kingdom*
[2]*Atominstitut, Technische Universität Wien, 1020 Vienna, Austria*
[3]*Institute for Theoretical Physics, ETH Zürich, Wolfgang-Pauli-Strasse 27, 8093 Zürich, Switzerland*
[4]*Department of Physics, University of Zurich, Winterthurerstrasse 190, 8057 Zurich, Switzerland*
[5]*Department of Materials, University of Oxford, Oxford OX1 3PH, United Kingdom*
[6]*Institute of Science and Technology Austria, Am Campus 1, 3400 Klosterneuburg, Austria*
[7]*L-NESS, Physics Department, Politecnico di Milano, via Anzani 42, 22100 Como, Italy*
[8]*IQOQI Vienna, Austrian Academy of Sciences, Boltzmanngasse 3, 1090 Vienna, Austria*
[9]*School of Physics, Trinity College Dublin, College Green, Dublin 2 D02 K8N4, Ireland*
[10]*Department of Physics, King's College London, Strand, London WC2R 2LS, United Kingdom*

(Received 3 March 2025; revised 4 July 2025; accepted 16 September 2025; published 14 November 2025)

We experimentally realize a quantum clock by using a charge sensor to count charges tunneling through a double quantum dot (DQD). Individual tunneling events are used as the clock's ticks. We quantify the clock's precision while measuring the power dissipated by the DQD and, separately, the charge sensor in both direct-current and radio-frequency readout modes. This allows us to probe the thermodynamic cost of creating ticks microscopically and recording them macroscopically. Our experiment is the first to explore the interplay between the entropy produced by a microscopic clockwork and its macroscopic measurement apparatus. We show that the latter contribution not only dwarfs the former but also unlocks greatly increased precision, because the measurement record can be exploited to optimally estimate time even when the DQD is at equilibrium. Our results suggest that the entropy produced by the amplification and measurement of a clock's ticks, which has often been ignored in the literature, is the most important and fundamental thermodynamic cost of timekeeping at the quantum scale.

DOI: 10.1103/5rtj-djfk

Clocks are physical systems tracking the passage of time, usually by quantifying time in discrete units called "ticks" which are stored in a register. In practice this may, for example, be the clock's hand counting pendulum oscillations [1,2], a digital counter counting laser oscillations in an atomic clock [3–5], or even the amount of extant carbon 14 in dead organic material counting decay events [1]. One property all clocks have in common is that they rely on entropy increase due to the second law of thermodynamics to create an irreversible record of how much time has passed [1,6–11]. For all practical purposes, a clock's counter thus always increases, which aligns with our experience that clocks always tick forward. In the microscopic realm, however, quantum phenomena generally produce orders of magnitude less entropy than classical processes, leading to stochastic fluctuations [12] that may cause a clock to tick backward on the quantum scale [13].

This behavior is exemplified in Fig. 1(a): a three-state system $(0, L, R)$ is the quantum clockwork (left), measurement apparatus (center), and the macroscopic agent (right). While the example is presented with incoherent semiclassical dynamics, the conclusions we draw also hold for an adaptation to coherent dynamics; see details in Supplemental Material (SM) [14]. In this example, the transition $0 \to L$ is driven by a hot thermal bath, $L \leftrightarrow R$ is balanced bidirectionally and does not rely on an external environment, $R \to 0$ is mediated by a cold thermal bath. Overall, the external environments induce a cycle $0 \to L \to R \to 0$ that transfers heat from hot to cold, producing entropy in accordance with the second law of thermodynamics. Considering these elementary cycles as ticks of the clock, the hot-cold bias drives the clock forward. Nevertheless, stochastic fluctuations may sometimes transfer heat against the thermal gradient, causing

*These authors contributed equally to this work.
†Contact author: vivek.wadhia@eng.ox.ac.uk
‡Contact author: florianmeier256@gmail.com
§Contact author: natalia.ares@eng.ox.ac.uk

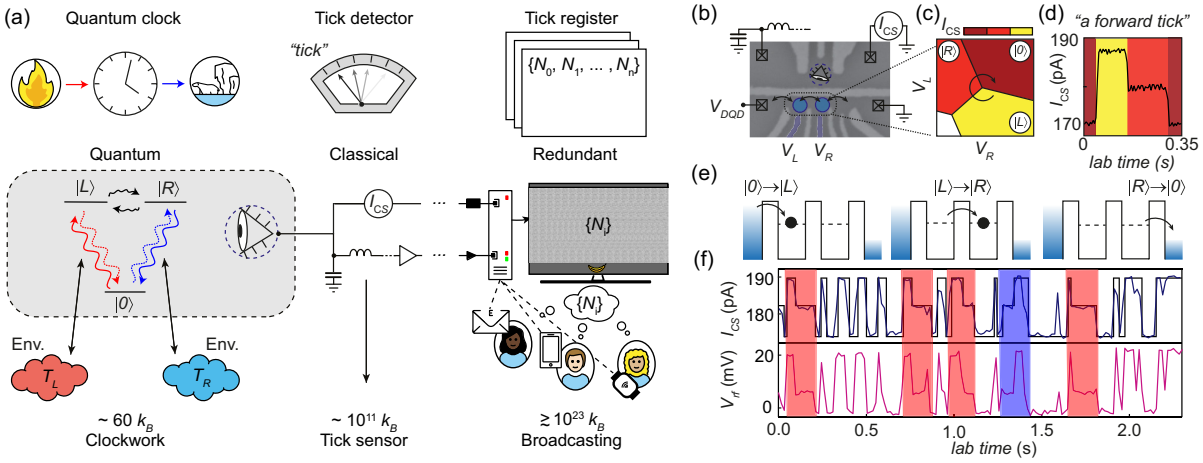


FIG. 1. Concept versus experiment. (a) A DQD with charge occupation states $|0\rangle, |L\rangle, |R\rangle$ stochastically exchanging charges with thermal environments can be used as a clock by identifying quantum jumps as *ticks* [experimentally $\sim 60 k_B$ per tick; see value estimated as a maximum from Fig. 2(a)]. Classically recording ticks to make them redundantly accessible for macroscopic agents requires measuring the quantum state and turning it into redundant information (right side). We found the cost of extraction to lie between $\sim 10^9 k_B$ and $\sim 10^{11} k_B$ per tick in our experiment, depending on the measurement method; see respective values shown in Figs. 2(b) and 2(c). Nevertheless, readout dissipation is several orders of magnitude smaller than macroscopic dissipation of the order $\gtrsim 10^{23} k_B$. (b) Scanning electron microscope image of a device similar to the one used in this experiment. Blue circles represent a DQD and the eye represents a charge sensor dot used for classical readout. $V_L$ and $V_R$ are the voltages applied to gate electrodes that control the number of charges within the left and right dot, respectively. Charge transport can occur from either source to drain, drain to source, or any intermediary process (black arced arrows), influenced by an applied source-drain voltage $V_{\mathrm{DQD}}$ across the DQD. (c) Sketch of a charge stability diagram. Intersection of charge occupation states $|0\rangle$, $|L\rangle$ and $|R\rangle$ is a triple point. Fluctuations about this point cause a cycling of states (black arrow) which correspond to a forward clock tick. (d) The simplest case of a forward clock tick measured with current in relation to lab time. The trace forms a discrete, three-level telegraph signal that corresponds to the charge occupation states in (c). (e) Schematic representation of the same forward clock tick as (d) in terms of charge transport. Initially, a charge enters from the source to the left dot $|0\rangle \rightarrow |L\rangle$, moves to the right dot $|L\rangle \rightarrow |R\rangle$, and finally moves to the drain $|R\rangle \rightarrow |0\rangle$. (f) Readout trace from both dc (top) and rf reflectometry (bottom), with respect to lab time. Black trace highlights the result of our level-identification algorithm. Shaded regions indicate ticks: red for forward and blue for backward.

the microscopic clock to tick backward. The extreme case being both baths are brought to the same temperature, where both tick directions are equally likely, no entropy is produced on average, and the clock stops ticking.

By continuously monitoring the microscopic clockwork, however, an observer could register each stochastic transition ($0 \rightarrow L, L \rightarrow 0$, etc.) as a new tick. This would restore the unidirectional flow of time recorded by the clock, even in the absence of a thermal gradient driving the clockwork. Yet a paradox arises: a clock is a manifestly irreversible device that distinguishes past from future—how can it produce no entropy? The resolution, as we verify in this Letter, is the measurement process itself produces entropy while creating a classical record of the quantum clock's ticks [25–33].

To demonstrate this, we experimentally realize the quantum-clock model of Fig. 1(a) using a double quantum dot (DQD). Ticking of this clock is probed via direct current (dc) and radio-frequency (rf) reflectometry readout modes, whose power dissipation can be directly inferred. We are thus able to measure two distinct sources of entropy production driving the clock: (1) the entropy produced by the quantized clockwork, and (2) the entropic cost of generating a classical measurement record. The first contribution has been the subject of several studies showing more regular ticks generally require more dissipation [6–8,10,11,13,32]. This principle is reminiscent of more general thermodynamic uncertainty relations (TURs). For classical stochastic systems [34–38] and quantum systems [39–46], TURs bound microscopic fluctuations by entropy production, though in certain settings the bounds are quite loose [2,47,48]. Nevertheless, our measurements show that the second contribution—the entropic cost of extracting classical ticks from the quantum clock—is, in fact, the dominant one by 9 orders of magnitude, highlighting the separation of scales between microscopic irreversibility and irreversibility induced by the measurement. We also show that exploiting all information in the measurement record to optimally estimate time [49], boosts the clock's precision by an order of magnitude compared to naively counting charge-transfer cycles.

*Experimental realization*—We realize a quantum clock using charge occupation states of a DQD. Charge transport through the DQD constitutes the ticking mechanism of the clock. A charge sensor dot, capacitively coupled to the DQD, is used to monitor the DQD, converting its charge

occupation state into a classical signal [50,51]. The quantum dots are defined electrostatically using a Ge/SiGe heterostructure with gate electrodes patterned on top [52], similar to Fig. 1(b). The semiconductor device was loaded into a dilution refrigerator and cooled down to $T = 180$ mK. Typical charging energies for these devices are ∼1.3 meV.

Transport of a charge between source and drain defines clock ticks. This process can be divided into three states, a charge in the left dot $|L\rangle$, a charge in the right dot $|R\rangle$, or no charge in either dot $|0\rangle$. A *forward* tick is any sequence that starts with $|0\rangle \to |L\rangle$ and ends with $|R\rangle \to |0\rangle$ with no $|0\rangle$ between. For example, $|0\rangle \to |L\rangle \to |R\rangle \to |0\rangle$ like in Fig. 1(e), but also $|0\rangle \to |L\rangle \to |R\rangle \to |L\rangle \to |R\rangle \to |0\rangle$, etc. A *backward* tick, conversely, is defined as starting with $|0\rangle \to |R\rangle$ and ending with $|L\rangle \to |0\rangle$ with no $|0\rangle$ between. Superpositions of DQD charge states are not considered as part of this experiment because they decohere faster than the measurement rate. Thus, the DQD is always in a definite charge occupation state when measured, which is not substantially impacted by the measurement. By applying a voltage bias across the double dot $V_{\mathrm{DQD}}$, we effectively have two thermal baths (given by source and drain reservoirs) out of equilibrium, and one of these tick processes becomes favored over the other. Each tick results in the dissipation of energy $q = e|V_{\mathrm{DQD}}|$, where $e$ is the elementary charge. For environments at inverse temperature $\beta$, this equals an entropic cost per tick,

$$\Sigma_{\mathrm{tick}} = \beta e|V_{\mathrm{DQD}}|. \tag{1}$$

In this experiment, we use two distinct methods to record ticks. Firstly, by measuring changes in the current flowing through the charge sensor dot (dc charge sensing). Secondly, through radio-frequency (rf) reflectometry that measures changes in the sensor's reflectance given a fixed rf input signal. Applying a voltage bias $V_{\mathrm{cs}}$ to the charge sensor generates a current $I_{\mathrm{cs}}$, that varies with the charge occupation of the DQD. Figure 1(d) shows an example of a dc measurement: three distinct current levels appear that correspond to $|0\rangle$, $|R\rangle$, and $|L\rangle$. Creating a classical record of the DQD state thus comes at a fundamental entropic cost due to the power dissipated through the sensor dot, given by Ohm's law $P^{\mathrm{dc}}_{\mathrm{diss}} = V_{\mathrm{cs}} I_{\mathrm{cs}}$. In order to lower the dissipation $V_{\mathrm{cs}}$ must be decreased. However this results in a decrease in $I_{\mathrm{cs}}$, which in turn decreases the signal-to-noise ratio (SNR). Qualitatively a lower SNR equates to less difference between the three levels of the telegraphic signal. Section B 3 of SM [14] provides a more detailed explanation.

For rf reflectometry, a reference signal with a fixed power $P_{\mathrm{in}}$ is sent to an rf cavity coupled to the charge sensor. It is then reflected back carrying information about the charge occupation state of the DQD. Using demodulation, traces like Fig. 1(f) can be obtained. The change in the reflected signal results in a reflected power $P_{\mathrm{out}}$, that is smaller in magnitude than $P_{\mathrm{in}}$. By accounting for known losses that occur in the signal chain, it is possible to compare these two quantities and establish the power dissipated across the sensor when using reflectometry. A more detailed description of this calculation is given in Sec. A 4 in SM [14]. To modulate the SNR, the input signal frequency $f_{\mathrm{rf}}$ was gradually increased, moving it progressively off-resonance with the rf cavity. As with dc measurements, this leads to a change in the power dissipated and hence the SNR.

*Experimental protocol*—$V_{\mathrm{DQD}}$ was initially set to 0 mV to simulate two baths in thermal equilibrium. $V_{\mathrm{cs}}$ was set to 0.345 mV. An rf signal was applied to the charge sensor, with frequency $f_{\mathrm{rf}} = 114$ MHz and power $P_{\mathrm{rf}} = -20$ dBm. These initial settings were chosen to optimize the SNR of the sensor signal. The acquisition card's integration time, both for the dc and rf sensor configurations, was set to 5 ms. A suitable triple point in the charge stability diagram was then selected such that transitions between states $|0\rangle$, $|L\rangle$, and $|R\rangle$ occur purely due to stochastic fluctuations. That is, the system was not driven by an external ac signal. Following this, transitions between these three states were slowed down until they appeared as a three-level telegraphic signal as in Fig. 1(f). This was achieved by gradually increasing the gate voltages controlling the tunnel barriers of the DQD, and estimating the tunneling rates (also referred to as jump rates) between the dots until they were all equal. Once suitable rates were achieved, these gate voltages remained fixed for the remainder of the experiment.

A 30-min measurement was then taken of the current through the charge sensor $I_{\mathrm{cs}}(t)$, and the reflected rf signal $V^{\mathrm{rf}}_{\mathrm{out}}(t)$. $I_{\mathrm{cs}}(t)$ and $V^{\mathrm{rf}}_{\mathrm{out}}(t)$ were filtered and amplified, with $V^{\mathrm{rf}}_{\mathrm{out}}(t)$ also demodulated, in order to obtain classical signals for readout. These signals were then used to identify clock ticks, as detailed in SM [14] Sec. A. From this data, it is possible to estimate the entropic cost of the clock ticking. In order to estimate and compare the entropic cost of the measurement process, the SNR needs to be modulated. This was achieved by decreasing $V_{\mathrm{cs}}$ from 0.345 to 0.102 mV while increasing $f_{\mathrm{rf}}$ from 114 to 128 MHz, in four steps. In other words, there are four settings of the SNR ranging from very good to very poor. The process of recording 30-min measurements was then repeated for each SNR setting. Finally, to simulate the effect of thermal baths out of equilibrium, $V_{\mathrm{DQD}}$ was changed from 0 to +1 mV for nine settings, with four SNR measurements taken at each value of $V_{\mathrm{DQD}}$.

*Theoretical description*—The present experiment can be described by a classical master equation [53,54],

$$\dot{\mathbf{p}} = M\mathbf{p}, \tag{2}$$

where $\mathbf{p} = (p_0, p_R, p_L)$ denotes charge state occupation probability, and $M$ the transition rate matrix. The validity of this model is discussed in Sec. C of SM [14]. Each experimental run yields a stochastic trajectory [55,56] of the master equation (2). In the readout signal $I_{\mathrm{cs}}(t)$, from either the dc or rf methods, the states $|0\rangle$, $|R\rangle$, and $|L\rangle$ manifest as three signal values $I_{\mathrm{l}} < I_{\mathrm{m}} < I_{\mathrm{h}}$. Due to noise, the signal does not exactly take one of the three values, moreover the three values are *a priori* unknown. Initially, the readout has to be calibrated by measuring the $I_{\mathrm{cs}}(t)$ for some time and creating a histogram of the measured values. For sufficiently high readout SNR, the histogram exhibits three distinct peaks centered on the values $I_{\mathrm{l/m/h}}$, where each peak is identified with one of the three microscopic states with an estimated identification error between 0.1% and 1% (see Fig. 6 and Sec. B in SM [14] for details). Through this identification, the measured signal $I_{\mathrm{cs}}(t)$ is converted into a sequence $S(t) \in \{0, R, L\}$ of states as shown in Fig. 1(f). While the signal analyzer includes a clock to assign time tags $t$ to the measured states, this is only required for calibration. To use the device as a clock, determining $t$ is the goal. Thus, only the instantaneous state $S(t)$ is required and not $t$. This is achieved by recording the sequence of charge occupation states occupied up to "$t$," starting with the initial state $s_0$, the state after the first jump $s_1$ and so on. We denote this sequence as $\mathbf{s}(t) = (s_0, s_1, \ldots, s_{m(t)})$, where $m(t)$ the number of jumps recorded.

*Time estimation*—The time estimator $\Theta_{\mathrm{net}}$ can be reconstructed based on the record $\mathbf{s}(t)$ by counting all the forward ticks as $+1$ and all the backward ticks as $-1$ toward the net number of transfers $N[\mathbf{s}(t)]$. Finally, $\Theta_{\mathrm{net}}[\mathbf{s}(t)] = \nu^{-1} N[\mathbf{s}(t)]$ is obtained by normalizing by the average charge transfer rate $\nu$, which can be initially calibrated to express $\Theta_{\mathrm{net}}$ in some reference unit, e.g., seconds. The uncertainty of the calibrated frequency can be made arbitrarily small by increasing the calibration time (Sec. B 2 of SM [14]).

While $\Theta_{\mathrm{net}}$ is how the ticks are naturally encoded in the charge environments, it is a suboptimal way of estimating time after readout where the full jump sequence $\mathbf{s}(t)$ is (classically) available. This becomes particularly apparent when considering the equilibrium case $V_{\mathrm{DQD}} \approx 0$ mV, where no net charge transfer takes place $N[\mathbf{s}(t)] \approx 0$ and the passage of time is not recorded microscopically. For stochastic evolution following Eq. (2), a theoretically optimal unbiased time estimator linear in the number of observed jumps exists [49]. Unbiased refers to the expectation value $\mathrm{E}[\Theta(t)] = t$ being equal to the lab time $t$, optimality to the precision defined in Eq. (4). This optimal choice is

$$\Theta_{\mathrm{opt}}[\mathbf{s}(t)] = \sum_{k=0}^{m(t)} \frac{1}{\Gamma_{s_k}} = \sum_{s \in \{0,R,L\}} \frac{n_s(t)}{\Gamma_s}, \tag{3}$$

$n_s(t)$ is the number of times the state $s$ appears in the sequence $\mathbf{s}(t)$. The sum weights each jump from a state $s$ by the average time it takes for the system to leave the state, which is given by $1/\Gamma_s = -1/M_{ss}$. Similar to the normalization $\nu$ for $\Theta_{\mathrm{net}}$, the rates $\Gamma_s$ can be initially calibrated with respect to a lab clock.

One way of quantifying the quality of the time estimate $\Theta$ is to compare the expectation value $\mathrm{E}[\Theta(t)]$ with the variance $\mathrm{Var}[\Theta(t)]$. We consider the precision

$$\mathcal{S} = \lim_{t \to \infty} \frac{\mathrm{E}[\Theta(t)]^2}{t \mathrm{Var}[\Theta(t)]}, \tag{4}$$

which captures the absolute timescale at which the estimator fluctuates in units of a rate, e.g., Hz. The larger the precision $\mathcal{S}$, the faster the process that can be estimated reliably with the clock (details in the End Matter). SM [14] includes pertinent detail how $\mathcal{S}$ is obtained empirically (Sec. B 2) and theoretically (Sec. C 4).

*Thermodynamic analysis*—In Fig. 2, precision $\mathcal{S}$ is plotted against the dissipation in the DQD in (a), the sensor dot for dc measurement in (b) and rf measurement in (c). The comparison in Fig. 2(a) reveals a trade-off between the dissipation $\Sigma_{\mathrm{tick}}$ in the clockwork and the precision of $\Theta_{\mathrm{net}}$. As expected, the precision of the microscopic time record vanishes when the DQD is brought to equilibrium. This is also in agreement with the TUR [34–38], which translates to $\mathcal{S} \leq \nu \Sigma_{\mathrm{tick}}/2$. Nevertheless, the optimal estimator $\Theta_{\mathrm{opt}}$ still works even when the clockwork is at equilibrium. Ultimately this is possible because of the dissipation required for the measurement to create the irreversible record of the equilibrium DQD dynamics. When the readout SNR is sufficiently high, as shown in Figs. 2(b) and 2(c), both $\Theta_{\mathrm{net}}$ and $\Theta_{\mathrm{opt}}$ yield high precision. However, when the measurement dissipation drops below a method dependent threshold, both time estimates become ill-defined and the clock stops ticking altogether.

*Discussion*—It is well established that quantum clocks produce entropy to generate the ticks necessary to measure time [1,6–11]. However, the critical role of measurement irreversibility in reading the clock's ticks has remained unexplored. Although a recent experiment has investigated measurement backaction on a quantum clock [57], our Letter is the first experiment probing the thermodynamic cost of this step. In doing so, we have demonstrated charge transport across a DQD can be used to construct a microscopic quantum clock, which is a key step towards building autonomous quantum machines [58–61].

In our experiment, we observed rf reflectometry is thermodynamically more efficient than dc measurement. For both methods, however, we found that dissipation is fundamentally linked to the SNR of the readout signal, and a minimum amount of dissipation is needed to create a classical record of the quantum ticks. While we confirmed the clock's precision is improved by increasing entropy

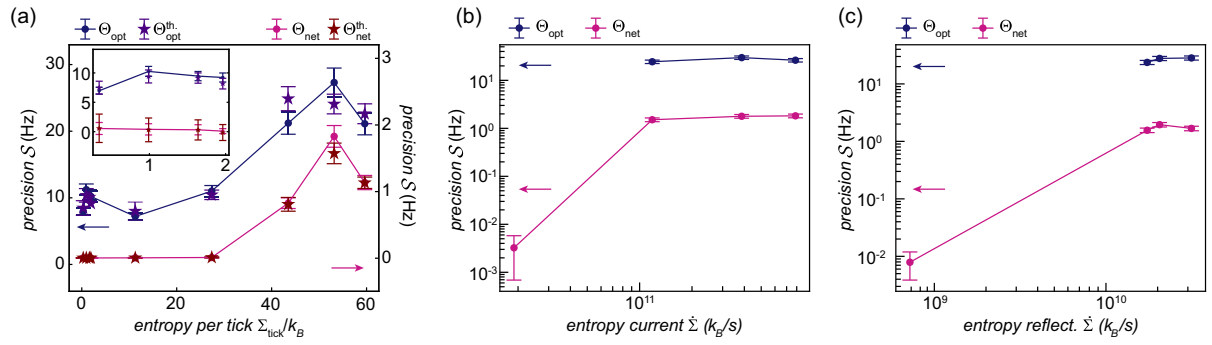


FIG. 2. Clock precision and entropy trade-off (empirical data and theory comparison). (a) Here, the precision $\mathcal{S}$ of the clock defined by the net number of charges $\Theta_{\mathrm{net}} = \nu^{-1}N(t)$ transported across the DQD is plotted against the entropy dissipated per tick (scale on the right). Furthermore, the normalized precision of the optimal estimator $\Theta_{\mathrm{opt}}$ from Eq. (3) is shown, also as a function of entropy per charge transport (scale on the left). The dots indicate empirical estimates for the precision (SM [14] Sec. B 2), and stars the theory prediction from the Markovian model (SM [14] Sec. C 4). Drifts in the device can lead to changes in the transition rates and ultimately deviations between theoretical and empirical values. (b) Data obtained with the dc measurement of the sensor dot showing how precision $\mathcal{S}$ for $\Theta_{\mathrm{net}}$ and $\Theta_{\mathrm{opt}}$ scales as a function of the dissipation rate in the sensor dot. (c) Data and dissipation for the reflectometry method, exhibiting three orders of magnitude lower dissipation than the dc method. Error bars show the estimated standard error as calculated in SM [14].

production in the clockwork, in accordance with previous work [1,6–11], this dissipation is eclipsed by the thermodynamic cost of the measurement. We have shown that the latter is particularly important for timekeeping because it can drive the clock's operation, even in scenarios where the clockwork itself ceases to generate entropy. While the model studied in this Letter is based on a DQD setup, extracting timing information from a quantum system generally comes at a thermodynamic cost, including in atomic or optical setups which currently form the basis of state-of-the-art clocks [3–5]. By establishing that tick extraction generally dominates the entropic cost of timekeeping, our Letter may guide future microscopic clock designs to improve their precision in the most thermodynamically efficient way.

*Acknowledgments*—The authors thank Georgios Katsaros for providing the device for this experiment, and Tony Apollaro, Ilia Khomchenko, and Gerard Milburn for discussions. V. W. acknowledges funding from UK Research and Innovation Grant No. EP/T517811/1. F. M., M. H., and P. E. acknowledge funding from the European Research Council (Consolidator Grant "Cocoquest" No. 101043705). M. H. and P. E. acknowledge funding from the Austrian Federal Ministry of Education, Science, and Research via the Austrian Research Promotion Agency (FFG) through Quantum Austria. R. S. acknowledges funding from the Swiss National Science Foundation via an Ambizione Grant No. PZ00P2_185986. M. T. M. is supported by a Royal Society University Research Fellowship. N. A. acknowledges support from the European Research Council (Grant Agreement No, 948932) and the Royal Society (No. URF-R1-191150). This project is cofunded by the European Union (Quantum Flagship project ASPECTS, Grant Agreement No. 101080167) and UK Research and Innovation (UKRI). Views and opinions expressed are however those of the authors only and do not necessarily reflect those of the European Union, Research Executive Agency, or UKRI. Neither the European Union nor UKRI can be held responsible for them.

F. M. analyzed the data and developed the theory framework with inputs from R. S., N. N., M. T. M., and P. E.; V. W. performed the experiment supervised by F. F. and with input from D. L. C.; D. J., J. S.-M. fabricated the device; A. B., D. C., and G. I. provided the heterostructure. F. M. drafted the initial version of the manuscript. V. W. wrote the experimental sections. M. H. conceptualized the narrative. M. T. M., P. E. and N. A. supervised the project. M. T. M., F. M., F. F., and N. A. conceived the original idea of the experiment. All authors contributed to the discussions of the results and finalization of the manuscript.

*Data availability*—The measurement traces as well as the code for analysis is publicly available on GitHub [62].

[1] G. J. Milburn, The thermodynamics of clocks, Contemp. Phys. **61**, 69 (2020).
[2] P. Pietzonka, Classical pendulum clocks break the thermodynamic uncertainty relation, Phys. Rev. Lett. **128**, 130606 (2022).
[3] A. D. Ludlow, M. M. Boyd, J. Ye, E. Peik, and P. O. Schmidt, Optical atomic clocks, Rev. Mod. Phys. **87**, 637 (2015).
[4] T. L. Nicholson, S. L. Campbell, R. B. Hutson, G. E. Marti, B. J. Bloom, R. L. McNally, W. Zhang, M. D. Barrett, M. S. Safronova, G. F. Strouse, W. L. Tew, and J. Ye, Systematic

evaluation of an atomic clock at $2 \times 10^{-18}$ total uncertainty, Nat. Commun. **6**, 6896 (2015).
[5] T. Bothwell, C. J. Kennedy, A. Aeppli, D. Kedar, J. M. Robinson, E. Oelker, A. Staron, and J. Ye, Resolving the gravitational redshift across a millimetre-scale atomic sample, Nature (London) **602**, 420 (2022).
[6] A. C. Barato and U. Seifert, Cost and precision of Brownian clocks, Phys. Rev. X **6**, 041053 (2016).
[7] P. Erker, M. T. Mitchison, R. Silva, M. P. Woods, N. Brunner, and M. Huber, Autonomous quantum clocks: Does thermodynamics limit our ability to measure time?, Phys. Rev. X **7**, 031022 (2017).
[8] A. N. Pearson, Y. Guryanova, P. Erker, E. A. Laird, G. A. D. Briggs, M. Huber, and N. Ares, Measuring the thermodynamic cost of timekeeping, Phys. Rev. X **11**, 021029 (2021).
[9] E. Schwarzhans, M. P. E. Lock, P. Erker, N. Friis, and M. Huber, Autonomous temporal probability concentration: Clockworks and the second law of thermodynamics, Phys. Rev. X **11**, 011046 (2021).
[10] A. P. T. Dost and M. P. Woods, Quantum advantages in timekeeping: Dimensional advantage, entropic advantage and how to realise them via Berry phases and ultra-regular spontaneous emission, arXiv:2303.10029.
[11] P. Pietzonka and F. Coghi, Thermodynamic cost for precision of general counting observables, Phys. Rev. E **109**, 064128 (2024).
[12] G. E. Crooks, Entropy production fluctuation theorem and the nonequilibrium work relation for free energy differences, Phys. Rev. E **60**, 2721 (1999).
[13] R. Silva, N. Nurgalieva, and H. Wilming, Ticking clocks in quantum theory, arXiv:2306.01829.
[14] See Supplemental Material at http://link.aps.org/supplemental/10.1103/5rtj-djfk, which includes Refs. [15–24].
[15] F. Vigneau, F. Fedele, A. Chatterjee, D. Reilly, F. Kuemmeth, M. F. Gonzalez-Zalba, E. Laird, and N. Ares, Probing quantum devices with radio-frequency reflectometry, Appl. Phys. Rev. **10**, 021305 (2023).
[16] A. Tharwat, Independent component analysis: An introduction, Appl. Comput. Inf. **17**, 222 (2021).
[17] G. Casella and R. Berger, *Statistical Inference* (Chapman and Hall/CRC, New York, 2024), 10.1201/9781003456285.
[18] P. Stein, A note on the volume of a simplex, Am. Math. Mon. **73**, 299 (1966).
[19] G. Schaller, *Open Quantum Systems Far from Equilibrium* (Springer International Publishing, New York, 2014).
[20] G. T. Landi and M. Paternostro, Irreversible entropy production: From classical to quantum, Rev. Mod. Phys. **93**, 035008 (2021).
[21] Y. Hasegawa, Quantum thermodynamic uncertainty relation for continuous measurement, Phys. Rev. Lett. **125**, 050601 (2020).
[22] T. Van Vu and K. Saito, Thermodynamics of precision in Markovian open quantum dynamics, Phys. Rev. Lett. **128**, 140602 (2022).
[23] S. V. Moreira, M. Radaelli, A. Candeloro, F. C. Binder, and M. T. Mitchison, Precision bounds for multiple currents in open quantum systems, Phys. Rev. E **111**, 064107 (2025).
[24] K. Macieszczak, Ultimate kinetic uncertainty relation and optimal performance of stochastic clocks, arXiv:2407.09839.
[25] L. Granger and H. Kantz, Thermodynamic cost of measurements, Phys. Rev. E **84**, 061110 (2011).
[26] K. Jacobs, Quantum measurement and the first law of thermodynamics: The energy cost of measurement is the work value of the acquired information, Phys. Rev. E **86**, 040106(R) (2012).
[27] S. Deffner, J. P. Paz, and W. H. Zurek, Quantum work and the thermodynamic cost of quantum measurements, Phys. Rev. E **94**, 010103(R) (2016).
[28] T. Debarba, G. Manzano, Y. Guryanova, M. Huber, and N. Friis, Work estimation and work fluctuations in the presence of non-ideal measurements, New J. Phys. **21**, 113002 (2019).
[29] Y. Guryanova, N. Friis, and M. Huber, Ideal projective measurements have infinite resource costs, Quantum **4**, 222 (2020).
[30] Y. Chu and J. Cai, Thermodynamic principle for quantum metrology, Phys. Rev. Lett. **128**, 200501 (2022); **128**, 200501(E) (2022); **129**, 109902(E) (2022).
[31] S. Dooley, M. J. Kewming, M. T. Mitchison, and J. Goold, Comment on "Thermodynamic principle for quantum metrology", arXiv:2205.11411.
[32] E. Schwarzhans, F. C. Binder, M. Huber, and M. P. E. Lock, Quantum measurements and equilibration: The emergence of objective reality via entropy maximisation, arXiv:2302.11253.
[33] C. L. Latune and C. Elouard, A thermodynamically consistent approach to the energy costs of quantum measurements, Quantum **9**, 1614 (2025).
[34] A. C. Barato and U. Seifert, Thermodynamic uncertainty relation for biomolecular processes, Phys. Rev. Lett. **114**, 158101 (2015).
[35] T. R. Gingrich, J. M. Horowitz, N. Perunov, and J. L. England, Dissipation bounds all steady-state current fluctuations, Phys. Rev. Lett. **116**, 120601 (2016).
[36] P. Pietzonka, F. Ritort, and U. Seifert, Finite-time generalization of the thermodynamic uncertainty relation, Phys. Rev. E **96**, 012101 (2017).
[37] K. Macieszczak, K. Brandner, and J. P. Garrahan, Unified thermodynamic uncertainty relations in linear response, Phys. Rev. Lett. **121**, 130601 (2018).
[38] J. M. Horowitz and T. R. Gingrich, Thermodynamic uncertainty relations constrain non-equilibrium fluctuations, Nat. Phys. **16**, 15 (2020).
[39] K. Ptaszyński, Coherence-enhanced constancy of a quantum thermoelectric generator, Phys. Rev. B **98**, 085425 (2018).
[40] B. K. Agarwalla and D. Segal, Assessing the validity of the thermodynamic uncertainty relation in quantum systems, Phys. Rev. B **98**, 155438 (2018).
[41] J. Liu and D. Segal, Thermodynamic uncertainty relation in quantum thermoelectric junctions, Phys. Rev. E **99**, 062141 (2019).
[42] G. Guarnieri, G. T. Landi, S. R. Clark, and J. Goold, Thermodynamics of precision in quantum nonequilibrium steady states, Phys. Rev. Res. **1**, 033021 (2019).
[43] A. Rignon-Bret, G. Guarnieri, J. Goold, and M. T. Mitchison, Thermodynamics of precision in quantum nanomachines, Phys. Rev. E **103**, 012133 (2021).
[44] K. Prech, P. Johansson, E. Nyholm, G. T. Landi, C. Verdozzi, P. Samuelsson, and P. P. Potts, Entanglement

and thermokinetic uncertainty relations in coherent mesoscopic transport, Phys. Rev. Res. **5**, 023155 (2023).
[45] G. Falasco, M. Esposito, and J.-C. Delvenne, Unifying thermodynamic uncertainty relations, New J. Phys. **22**, 053046 (2020).
[46] Y. Hasegawa, Thermodynamic uncertainty relation for general open quantum systems, Phys. Rev. Lett. **126**, 010602 (2021).
[47] K. Brandner, T. Hanazato, and K. Saito, Thermodynamic bounds on precision in ballistic multiterminal transport, Phys. Rev. Lett. **120**, 090601 (2018).
[48] M. Gerry and D. Segal, Absence and recovery of cost-precision tradeoff relations in quantum transport, Phys. Rev. B **105**, 155401 (2022).
[49] K. Prech, G. T. Landi, F. Meier, N. Nurgalieva, P. P. Potts, R. Silva, and M. T. Mitchison, Optimal time estimation and the clock uncertainty relation for stochastic processes, Phys. Rev. X **15**, 031068 (2025).
[50] T. Nakajima, Y. Kojima, Y. Uehara, A. Noiri, K. Takeda, T. Kobayashi, and S. Tarucha, Real-time feedback control of charge sensing for quantum dot qubits, Phys. Rev. Appl. **15**, L031003 (2021).
[51] J. M. Elzerman, R. Hanson, J. S. Greidanus, L. H. Willems van Beveren, S. De Franceschi, L. M. K. Vandersypen, S. Tarucha, and L. P. Kouwenhoven, Few-electron quantum dot circuit with integrated charge read out, Phys. Rev. B **67**, 161308(R) (2003).
[52] M. Ciorga, A. S. Sachrajda, P. Hawrylak, C. Gould, P. Zawadzki, S. Jullian, Y. Feng, and Z. Wasilewski, Addition spectrum of a lateral dot from Coulomb and spin-blockade spectroscopy, Phys. Rev. B **61**, R16315 (2000).
[53] G. B. Cuetara and M. Esposito, Double quantum dot coupled to a quantum point contact: A stochastic thermodynamics approach, New J. Phys. **17**, 095005 (2015).
[54] L. P. Bettmann, M. J. Kewming, and J. Goold, Thermodynamics of a continuously monitored double-quantum-dot heat engine in the repeated interactions framework, Phys. Rev. E **107**, 044102 (2023).
[55] C. Van den Broeck and M. Esposito, Ensemble and trajectory thermodynamics: A brief introduction, Physica (Amsterdam) **418A**, 6 (2015).
[56] H. Carmichael, *An Open Systems Approach to Quantum Optics* (Springer, Berlin Heidelberg, 1993).
[57] X. He, P. Pakkiam, A. A. Gangat, M. J. Kewming, G. J. Milburn, and A. Fedorov, Effect of measurement back-action on quantum clock precision studied with a superconducting circuit, Phys. Rev. Appl. **20**, 034038 (2023).
[58] F. Meier, M. Huber, P. Erker, and J. Xuereb, Autonomous quantum processing unit: What does it take to construct a self-contained model for quantum computation?, arXiv:2402.00111.
[59] M. P. Woods, Quantum frequential computing: A quadratic run time advantage for all algorithms, arXiv:2403.02389.
[60] D. Cilluffo, L. Lautenbacher, G. Spaventa, S. F. Huelga, and M. B. Plenio, Physically constrained quantum clock-driven dynamics, arXiv:2409.02857.
[61] J. A. Marín Guzmán, P. Erker, S. Gasparinetti, M. Huber, and N. Yunger Halpern, Key issues review: Useful autonomous quantum machines, Rep. Prog. Phys. **87**, 122001 (2024).
[62] V. Wadhia, F. Meier, F. Fedele, and D. Craig, Data and code, https://github.com/aspects-quantum/equilibrium-clock-public (2025).
[63] D. Craig, Inference of transport phenomena in quantum devices, Ph. D. thesis, University of Oxford, 2023.
[64] M. P. Woods, R. Silva, and J. Oppenheim, Autonomous quantum machines and finite-sized clocks, Ann. Henri Poincaré **20**, 125 (2019).
[65] M. P. Woods, Autonomous ticking clocks from axiomatic principles, Quantum **5**, 381 (2021).
[66] Mischa P. Woods, R. Silva, G. Pütz, S. Stupar, and R. Renner, Quantum clocks are more accurate than classical ones, PRX Quantum **3**, 010319 (2022).
[67] D. Nello and A. Silva, Powering a quantum clock with a non-equilibrium steady state, arXiv:2412.13107.
[68] G. T. Landi, M. J. Kewming, M. T. Mitchison, and P. P. Potts, Current fluctuations in open quantum systems: Bridging the gap between quantum continuous measurements and full counting statistics, PRX Quantum **5**, 020201 (2024).
[69] D. R. Cox, *Renewal Theory* (Methuen & Co Ltd, London, 1962).

## End Matter

*Tick identification method*—Here, we provide pertinent detail regarding our method to identify ticks from the measurement signal. To create a classical record of the DQD clock's ticks, the two measurement signals obtained through either the dc or rf sensor method have to be postprocessed to infer the state of the DQD. In Fig. 3, we show a comparison of a current signal $I_{\mathrm{cs}}(t)$ (dc), with the rf sensor voltage $V_{\mathrm{Y}}^{\mathrm{rf}}(t)$ (rf). The signal $V_{\mathrm{Y}}^{\mathrm{rf}}$ is the Y quadrature component of the rf signal measured with an rf lock-in amplifier after demodulation, chosen for illustration purposes (details in Sec. A 3 of SM [14]). From comparison of Fig. 3(b) versus Fig. 3(d), it can be seen that both readout methods yield qualitatively similar outputs, up to a difference in noise characteristics. Still, both outputs can then be used to infer the state of the DQD by identifying the three separated levels around which the signals fluctuate. We use the following method to identify the three levels from the given signal (further details in Sec. B 1 of SM [14]).

Initially, the output signals have to be calibrated to determine the three values $I_{\mathrm{l}} < I_{\mathrm{m}} < I_{\mathrm{h}}$. In the following, we describe the identification method for the dc sensor readout, but the method works analogously for the voltage output from the rf reflectometry. In principle, one way to calibrate the readout is to initially run the device for some

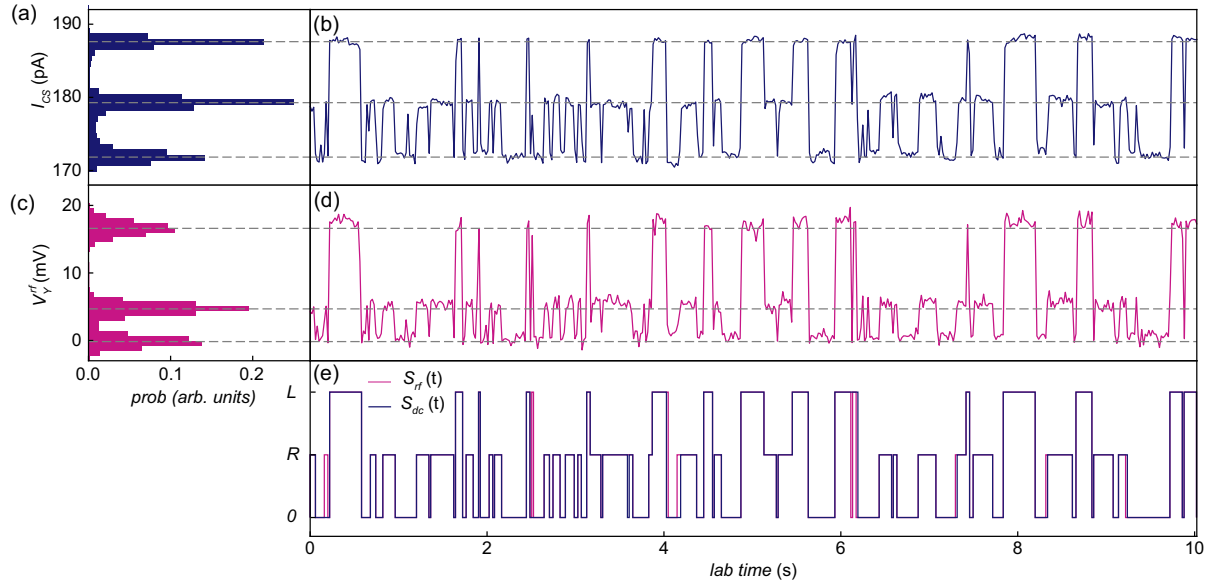


FIG. 3. Measurement traces of length 10 s using both the dc (b) and the rf reflectometry method (d). The trace is taken for a DQD bias $V_{\mathrm{DQD}} = 0$ mV, a sensor dot bias $V_{\mathrm{cs}} = 0.345$ mV, and frequency $f_{\mathrm{rf}} = 114$ MHz for the rf reflectometry drive. (a) Histogram $p(I)$ of the current values for the full 30 min data trace showing the emergence of three peaks corresponding to the DQD charge occupation states, shown as the dashed lines. (c) Analogously, the histogram $p(V)$ for the demodulated Y-component of rf sensor signal is shown here (details in Sec. A 3 of SM [14]). (e) The discretized signal $S(t)$ for both the dc and rf reflectometry methods, obtained from the measurement traces by identifying one of the three states from the noisy signal. For most times, the discretized signals from the two readout methods agree with each other. In general, rf is more sensitive than dc sensing, leading to instances where the two discretized signals are not exactly identical. Nevertheless, as can be seen, this difference does not significantly affect level identification.

time and create a histogram $p(I)$ for how likely a given output current value is. From the histogram, three peaks then reveal the three current values corresponding to the three states of the DQD. After the initial calibration, the output signal can then be converted in real time into a discrete output encoding the DQD state, from which the clock's ticks can then be inferred.

Instead of a real-time identification, we have analyzed the present experiment's output *a posteriori*. For each of the 30 min data traces, we create a histogram for the output current values, shown in Fig. 3(a), or, respectively, voltage values shown in Fig. 3(c). Based on the method from [63], we numerically fit three Gaussian peaks $\sum_{i=1}^{3} h_i \mathcal{N}(\mu_i, \sigma_i)$ to the histogram, where $\mu_i$ is the mean and $\sigma_i$ the width of the $i$th Gaussian. The prefactor $h_i$ are weights to account for the relative probability of each of the three levels. From the fitted normal distributions, the measurement output can then be converted into the discrete signal shown in Fig. 3(e), by mapping the current values $I_{\mathrm{cs}}(t)$ [or voltages $V^{\mathrm{rf}}(t)$] to the most likely of the three peaks from the histogram.

*Relating different notions of clock precision*—In the following paragraphs we provide details for how different notions for clock precision in the literature are related to the definition of $\mathcal{S}$ in Eq. (4). There are three distinct ways to characterize a ticking clock's output.

Time between ticks: If the clock's tick counter only increases, i.e., there are only forward ticks, one may consider the probability density $P[T = \tau]$ that the time between two subsequent ticks is $\tau \geq 0$ (the *waiting-time distribution*). In the literature [7,10,32,64–67] the *accuracy* with which such a tick estimates the underlying parameter time is defined by

$$\mathcal{N}_\infty = \frac{\mathrm{E}[T]^2}{\mathrm{Var}[T]}. \tag{B1}$$

If the ticks are independently and identically distributed (iid), making the clock a *renewal process*, the accuracy $\mathcal{N}_\infty$ can be understood as the expected number of times the clock ticks until it goes wrong by one tick. It is thus the precision of the clock relative to its own timescale, and $\mathcal{N}_\infty$ is timescale invariant.

Counting of ticks: When the number of ticks $N(t)$ is made up of forward ticks $N^+(t)$ and backward ticks $N^-(t)$ like for the DQD clock, the tick counter can sometimes jump backward or forward. As a result, there is no longer a unique waiting time describing a strictly increasing counter. By working in the framework of counting observables, one can thus consider the net number of ticks $N(t)$ instead of the waiting times. In this case, one defines the precision of the counting observable $N(t)$, also known in the literature as the Fano factor [6,34],

$$\mathcal{N} = \lim_{t\to\infty} \frac{\mathrm{E}[N(t)]}{\mathrm{Var}[N(t)]}. \tag{B2}$$

This is well defined thanks to the following generalized relations [49,68]:

$$\mathrm{E}[N(t)] = \nu t + O(1), \qquad \mathrm{Var}[N(t)] = Dt + O(1), \tag{B3}$$

with $\nu$ the tick rate and $D$ the diffusion constant. The Fano factor is time invariant and is thus also a measure of relative precision.

If the clock is a renewal process (ticks are iid and only forward), then it is possible to relate the moments of the tick time to the moments of the tick number in the long-time limit [13,69],

$$E[T] = \frac{1}{\nu}, \qquad \mathrm{Var}[T] = \frac{D}{\nu^3}. \tag{B4}$$

Thus, Eq. (B4) guarantee that for a renewal process the accuracy (B1) in the waiting time picture equals the precision from Eq. (B2), that is, $\mathcal{N} = \mathcal{N}_\infty$.

Time estimator from detailed jumps: Finally, one may construct a linear time estimator $\Theta(t)$ from the number of each type of tick that the clock produces (details in SM [14], Sec. D), which is assumed to be unbiased, i.e., $\mathrm{E}[\Theta(t)] = t + O(1)$. Following [49], we have defined the *absolute precision* $\mathcal{S}$, given by Eq. (4) in the main text and repeated here for convenience:

$$\mathcal{S} = \lim_{t\to\infty} \frac{\mathrm{E}[\Theta(t)]^2}{t\mathrm{Var}[\Theta(t)]}. \tag{B5}$$

To understand the terminology of absolute precision, note that in the number-of-ticks picture one could define an unbiased time estimator as $\Theta_{\mathrm{net}}(t) = \nu^{-1}N(t)$, in which case the two notions of precision $\mathcal{S}$ and $\mathcal{N}$ are related by

$$\mathcal{N} = \frac{\mathcal{S}}{\nu}. \tag{B6}$$

That is, the *relative precision* $\mathcal{N}$ equals the absolute precision $\mathcal{S}$ normalized by the clock's resolution $\nu$. This equality can be generalized even for time estimators such as the optimal estimator $\Theta_{\mathrm{opt}}(t)$ as discussed in Ref. [49], though in that case, there is in general no well-defined integer number of ticks $N(t)$, because the different increments of $\Theta_{\mathrm{opt}}(t)$ are not necessarily integer multiples of each other.

In summary, the relative precision is the clock's precision with respect to its own timescale, while the absolute precision is the precision relative to a fundamental unit of time.